A&A 394, 927–941 (2002)
DOI: 10.1051/0004-6361:20021157

Astronomy & Astrophysics

HIPPARCOS age-metallicity relation of the solar neighbourhood disc stars⋆

A. Ibukiyama[1] and N. Arimoto[1,2]

[1] Institute of Astronomy (IoA), School of Science, University of Tokyo, 2-21-1 Osawa, Mitaka, Tokyo 181-0015, Japan
[2] National Astronomical Observatory, 2-21-1 Osawa, Mitaka, Tokyo 181-8588, Japan

Received 12 December 2000 / Accepted 28 June 2002

Abstract. We derive age-metallicity relations (AMRs) and orbital parameters for the 1658 solar neighbourhood stars to which accurate distances are measured by the *HIPPARCOS* satellite. The sample stars comprise 1382 thin disc stars, 229 thick disc stars, and 47 halo stars according to their orbital parameters. We find a considerable scatter for thin disc AMR along the one-zone Galactic chemical evolution (GCE) model. Orbits and metallicities of thin disc stars show now clear relation each other. The scatter along the AMR exists even if the stars with the same orbits are selected. We examine simple extension of one-zone GCE models which account for inhomogeneity in the effective yield and inhomogeneous star formation rate in the Galaxy. Both extensions of the one-zone GCE model cannot account for the scatter in age – [Fe/H] – [Ca/Fe] relation simultaneously. We conclude, therefore, that the scatter along the thin disc AMR is an essential feature in the formation and evolution of the Galaxy. The AMR for thick disc stars shows that the star formation terminated 8 Gyr ago in the thick disc. As already reported by Gratton et al. (2000) and Prochaska et al. (2000), thick disc stars are more Ca-rich than thin disc stars with the same [Fe/H]. We find that thick disc stars show a vertical abundance gradient. These three facts, the AMR, vertical gradient, and [Ca/Fe]–[Fe/H] relation, support monolithic collapse and/or accretion of satellite dwarf galaxies as likely thick disc formation scenarios.

Key words. stars: abundances – stars: distances – Galaxy: abundances – Galaxy: evolution – Galaxy: solar neighbourhood – Galaxy: kinematics and dynamics

1. Introduction

The individual ages for solar neighbourhood stars are indispensable in the research of star formation history of the Galaxy. Twarog (1980) first derived the age-metallicity relation (AMR) for the disc in the neighbourhood of the Sun from *ubvy* and Hβ photometry of a large sample of field stars. Theoretical isochrones used in the age determination were taken from Ciardullo & Demarque (1977). In the Twarog's AMR, the metallicity increases from [Fe/H] = −1.0 at 13 Gyr to [Fe/H] = −0.03 at the age of the Sun. The mean metallicity has increased more slowly since then to a present value of [Fe/H] = +0.01 for the youngest stars. The dispersion in [Fe/H] is as small as ±0.1 dex at any given age. Carlberg et al. (1985) used stellar models of VandenBerg (1983) and a revised metallicity calibration that takes into account a temperature dependence. Both ages and metallicities were estimated in a photometric manner, and the resulting AMR is qualitatively similar to that of Twarog (1980), but [Fe/H] increases more gradually, showing an increase of only 0.3 dex over the past 15 Gyrs (cf. Nissen & Schuster 1991). The metallicity dispersion decreases from ±0.15 dex for the oldest stars (13−20 Gyrs) to ±0.05 dex for younger stars.

Edvardsson et al. (1993) derived elemental abundances of O, Na, Mg, Al, Si, Ca, Ti, Fe, Ni, Y, Zr, Ba, and Nd for 189 nearby long-lived disc dwarfs by using high resolution, high S/N, spectroscopic data. Individual ages were derived photometrically from fits in the $\log T_{\rm eff} - \log g$ plane of the isochrones by VandenBerg (1985). The uncertainties in the relative ages are about 25%. Due to metallicity measurements of high precision, Edvardsson et al. (1993) improved greatly the AMR, but ironically the resulting AMR clearly indicated a considerable scatter (∼0.15 dex) in the metallicities of disc stars formed at any given time, implying that there is only a very weak correlation between age and metallicity. The scatter seems to be substantially larger than that can be explained by observational errors. If the scatter is real, it would cause a serious difficulty for galactic chemical evolution (GCE) models, because it is easy to fit the average run of the data, but difficult to explain such a large scatter without breaking some of assumptions that GCE models usually make (Pagel & Tautvaišienė 1995).

Send offprint requests to: A. Ibukiyama,
e-mail: aibukiya@optik.mtk.nao.ac.jp

⋆ Tables 2 and 3 are only available in electronic form at the CDS via anonymous ftp to cdsarc.u-strasbg.fr (130.79.128.5) or via http://cdsweb.u-strasbg.fr/cgi-bin/qcat?J/A+A/394/927

Edvardsson et al. (1993) suggested that the scatter arises from star formation stimulated from sporadic episodes of gas infall, although it is also possible that a different rate of chemical enrichment, depending on the distance from the Galactic centre, causes a scatter of this kind.

In this article, we derived the ages and orbital parameters for 1658 solar neighbourhood stars, almost ten times more than previous researches. Hence we succeed in finding out new features of the Galaxy using stellar ages, chemical components, and orbits. The article is organised as follows. Section 2 derives the ages and the orbital parameters for sample stars. Section 3 shows the features relevant to thin disc stars while Sect. 4 shows those of thick disc. Section 5 discusses observational error in our data, abundance gradients, the abundance distribution functions, the formation of thick disc, and the scatter along the thin disc AMR. Section 6 concludes the present study.

2. The data

2.1. The observational data

2.1.1. Absolute magnitudes and colours

Visual magnitudes, $B-V$ colours, and parallaxes of nearby field stars were all taken from the *HIPPARCOS* catalogue (ESA 1997). The absolute magnitudes, M_{V_0}, and unreddened colours, $(B-V)_0$, were then calculated by applying the reddening corrections given by the model of Arenou et al. (1992). Certain number of stars in the *HIPPARCOS* catalogue suffer from uncertainties in parallaxes, binarities, and variabilities. Thus, the following criteria were introduced in our sample selection: (1) $\sigma_\pi/\pi < 0.1$, where π and σ_π are the parallax and the dispersion, respectively; (2) no binaries – binaries were excluded if explicitly identified in the *HIPPARCOS* catalogue; (3) non-variables – variables were excluded if assigned in the *HIPPARCOS* catalogue or in the [Fe/H] catalogue of Cayrel de Strobel et al. (2001); (4) no giants – giants were excluded according to their location on the CM diagram; LK bias (Lutz & Kelker 1973) was not corrected because Carretta et al. (1999) has shown recently that the bias is negligible if a strict sample selection ($\sigma_\pi/\pi < 0.12$) is applied (see also Ng & Bertelli 1998).

2.1.2. Metallicities

The stellar metallicities for F, G, and K stars were taken from the latest [Fe/H] catalogue of Cayrel de Strobel et al. (2001) which compiles the [Fe/H] values derived from high S/N and high resolution spectra. We cross-identified the *HIPPARCOS* catalogue and the [Fe/H] catalogue to derive a set of reliable M_{V_0}, $(B-V)_0$, and [Fe/H] for 429 stars. When several [Fe/H] values were given in the [Fe/H] catalogue, we adopted the newest observation. Since we wish to use preferentially the CCD data, we excluded the [Fe/H] data before 1985.

Additionally we took *ubvy*-Hβ photometry for F and G stars from the catalogue of Hauck & Mermilliod (1998). We calculated [Fe/H] from these data adopting the calibration by Schuster & Nissen (1989). We define the AMR using spectroscopic metallicity of Cayrel de Strobel et al. (2001) as "spectroscopic AMR" and the AMR using photometric metallicity derived from the data of Hauck & Mermilliod (1998) as "photometric AMR" hereafter.

Abundances of Ca were taken from Boesgaard & Tripicco (1986), Smith & Lambert (1986), Smith & Lambert (1987), Hartmann & Gehren (1988), Abia et al. (1988), Magain (1989), Cayrel de Strobel & Bentolila (1989), Gratton & Sneden (1991), Berthet (1991), Edvardsson et al. (1993), Pilachowski et al. (1993), Smith et al. (1993), Nissen et al. (1994), Beveridge & Sneden (1994), Nissen & Schuster (1997), Tomkin et al. (1997), Carney et al. (1997), Castro et al. (1997), Giridhar et al. (1997), Gonzalez (1998), Feltzing & Gustafsson (1998), King et al. (1998), Jehin et al. (1999), Clementini et al. (1999), Sadakane et al. (1999), Santos et al. (2000), Thorén & Feltzing (2000), Chen et al. (2000), Gonzalez & Laws (2000), and Fulbright (2000). Ca abundances may be less accurate than Fe abundances, for the number of Ca lines used in data reduction is fewer than that of Fe.

2.1.3. The kinematic data

We adopted radial velocities from the *HIPPARCOS* Input Catalogue (Turon et al. 1993), Barbier-Brossat et al. (1994), Duflot et al. (1995), and Malaroda et al. (2001). Proper motions were taken from the *HIPPARCOS* Catalogue. The space motions relative to the Sun, (U,V,W), were calculated using Johnson & Soderblom (1987); Edvardsson et al. (1993).

We obtained 4240 sample stars by cross checking *HIPPARCOS* data, [Fe/H] or *ubvy*-Hβ catalogue, and radial velocity catalogue. From 4240 whole sample, 1380 stars of poor parallax data, 1311 binaries, 428 variables, 1252 giants, and 133 stars observed before 1985 were excluded. In total, 1658 stars remained as our sample including 489 stars with spectroscopic [Fe/H] and 1169 stars with photometric [Fe/H]. [Ca/Fe] values were obtained for 277 stars among them.

Figure 1 shows the distances from the Sun of the sample stars. The sample stars are currently locating at the distances from 10 pc to 120 pc with a median value of 40 pc.

2.2. The analysis

2.2.1. Ages

Once M_{V_0}, $(B-V)_0$, and [Fe/H] were known, it was direct to derive ages of the selected stars by using the isochrone fitting. We adopted Yonsei-Yale isochrones (Yi et al. 2001), which were calculated with new OPAL opacities and Kurucz model atmospheres for a set of metallicities $Z = 0.00001$, 0.0001, 0.0004, 0.001, 0.004, 0.007, 0.01, 0.02 (solar), 0.04, 0.06, 0.08 and ages from $t = 1.0$ Gyr to 20.0 Gyr with an interval of $\Delta t = 1.0$ Gyr. The mixing length and helium enrichment rate were fixed to $\alpha \equiv l/H_\mathrm{p} = 1.7$ and $\Delta Y/\Delta Z = 2$, respectively, while no convective overshooting was introduced. Since Yonsei-Yale isochrones were calculated for Z instead of [Fe/H], we converted [Fe/H] of the selected stars into Z by using an empirical relation for the solar neighbourhood stars (Clementini et al. 1999):

$$\log(Z/Z_\odot) \simeq [\alpha/\mathrm{H}] \simeq \begin{cases} [\mathrm{Fe/H}] + 0.4, & [\mathrm{Fe/H}] \le -1.0 \\ 0.6[\mathrm{Fe/H}], & [\mathrm{Fe/H}] \ge -1.0 \end{cases} \quad (1)$$

Table 1. The sample stars.

	thin disc	thick disc	halo	total
photometric [Fe/H]	1010	143	16	1169
spectroscopic [Fe/H] (without [Ca/Fe])	173	28	11	212
spectroscopic [Fe/H] (with [Ca/Fe])	199	58	20	277
total	1382	229	47	1658

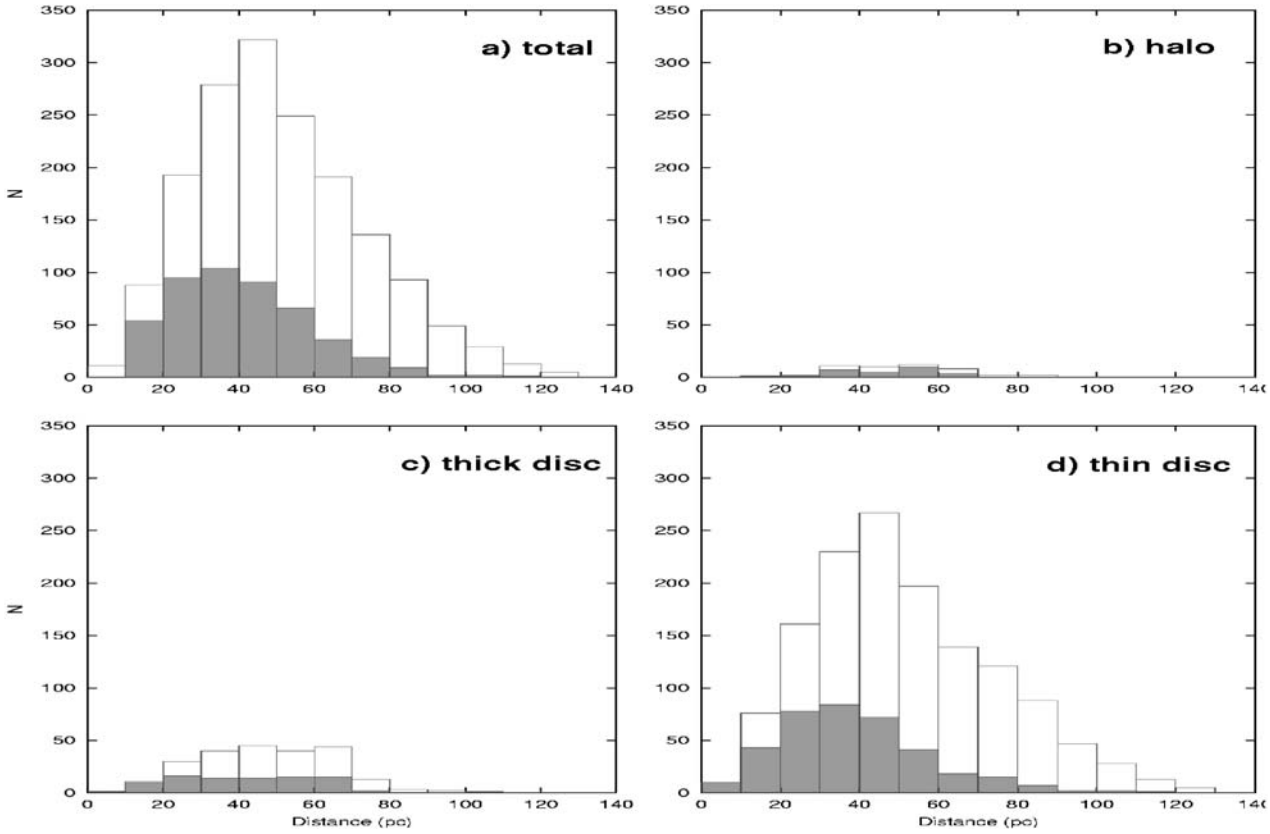

Fig. 1. The distribution of distances of the sample stars from the sun. **a)** Whole 1658 stars. **b)** 47 halo stars. **c)** 229 thick disc stars. **d)** 1382 thin disc stars. Gray boxes show the stars with spectroscopic data while open boxes represent the stars with photometric data.

where $Z_\odot = 0.02$, and α elements are assumed to dominate Z. Admittedly, this is rather a crude approximation, but it would not introduce significant effects on the resulting AMR and, we believe, is far better than a simple assumption of $\log(Z/Z_\odot) =$ [Fe/H]. We also calculated ages of the sample stars with the assumption of $\log(Z/Z_\odot) =$ [Fe/H] to find that the resulting ages are systematically older by ~0.2 dex for metal-poor stars ([Fe/H] ≤ -1). The difference becomes smaller toward higher [Fe/H].

Finally, knowing Z for the star, we interpolated the isochrones in $\log Z$ with the two adjacent metallicities and derived a set of isochrones with Z and ages from 1.0 to 20.0 Gyr. As illustrated in Fig. 2, the stellar age was derived by interpolating linearly the nearest two grid points of the isochrones on the $M_{V_0} - (B-V)_0$ diagram. Uncertainties in M_{V_0}, $(B-V)_0$, and Z cause errors for resulting ages. Errors in parallax of 10%, $(B-V)_0$ of 0.02 mag, and metallicity of 0.1 dex result in uncertainties in age of 0.064 dex, 0.073 dex, 0.082 dex, respectively. Thus a 0.12 dex age error exists for our sample on average.

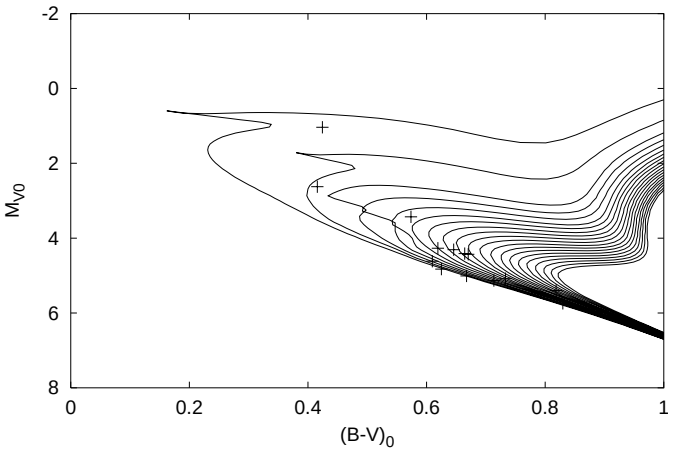

Fig. 2. The sample of isochrone fitting. Crosses represent solar metallicity stars ($0.0 \leq$ [Fe/H] < 0.005) while solid lines represent the isochrones for solar metallicity stars from 1 Gyr (top left) to 20 Gyr (bottom right).

2.2.2. The Galactic orbital parameters

We examined kinematics of the sample stars and calculated their orbital parameters in a similar way to Edvardsson et al. (1993) and Nissen & Schuster (1997).

We integrated their orbit backward in time by using a four-component Miyamoto-Nagai potential model including thin disc, thick disc, bulge, and halo (Sofue 1996). Integration was done using 6th order Symplectic formula with a constant time step of 10^5 year. We adopted the correction for the solar velocity of $(U_\odot, V_\odot, W_\odot) = (-10, 232, 6)\,\mathrm{km\,s^{-1}}$. The galactocentric distance and circular velocity of the sun were fixed to be 8.0 kpc and $226.0\,\mathrm{km\,s^{-1}}$, respectively (Edvardsson et al. 1993). Energy and angular momentum of the sample stars were conserved within an accuracy of 10^{-8}. We derived apogalactocentric distance projected to the Galactic plane, R_a, perigalactocentric distance, R_p, and maximum deviation from the plane, z_max. We also derived eccentricity, $e \equiv (R_\mathrm{p} - R_\mathrm{a})/(R_\mathrm{p} + R_\mathrm{a})$, and mean distance, $R \equiv (R_\mathrm{p} + R_\mathrm{a})/2$. Tables 2 and 3 give the orbital parameters of the sample stars.

We identified the populations of stars by using their rotational velocities, V, with respect to the Galaxy centre. The stars with $V \geq -62\,\mathrm{km\,s^{-1}}$, $-182\,\mathrm{km\,s^{-1}} \leq V < -62\,\mathrm{km\,s^{-1}}$, and $V < -182\,\mathrm{km\,s^{-1}}$ are assigned as thin disc, thick disc, and halo stars, respectively. Following Carney et al. (1989) and Prochaska et al. (2000), stars with $z_\mathrm{max} > 600$ pc are identified to be thick disc component even if their rotational velocities, V, are larger than $170\,\mathrm{km\,s^{-1}}$ in addition.

In our 1658 sample stars, we identified 1138 thin disc stars, 229 thick disc stars, and 47 halo stars.

The identified stellar populations are listed in Tables 2 and 3. Figures 3 show the CM diagrams of the whole sample with [Fe/H] measurements before sample selection (4240 stars), the selected 1138 thin disc stars, 229 thick disc stars, and 47 halo stars, respectively.

Thin disc stars rotate, in average, around the Galactic centre every 0.2 Gyr. For example, a 10 Gyr old star has rotated 50 times till now. Figures 4 show the snapshots of the orbit of our sample stars when we integrate their orbit backward to 0.2 Gyr and 2 Gyr. In the top two figures, the majority of stars rotate almost once. On such a short time scale, the orbits did not deviate so much and the similarities preserved. In the bottom figures, in which the orbits were integrated for 2 Gyr, however, the stars rotate for such long times that they are uniformly distributed in the torus because of their random motion. As a result, the sample stars older than 2 Gyr trace the star formation history in the various region in the torus, in spite of the fact that they now exist in the region within 100 pc from the sun. Hereafter, we define this region as the solar torus in which the "solar neighbourhood stars" formed in the past. Our sample stars reflect the star formation history not in the narrow sphere with a radius of 100 pc but in the wide torus region whose radius is 6 kpc $\sim$ 9 kpc from the Galactic centre described in Fig. 4.

3. The thin disc

3.1. The thin disc AMR

Figure 5 shows the spectroscopic AMR and the photometric AMR of thin disc stars. The line represents the GCE model by Pagel & Tautvaišienė (1995), which includes delayed elements production by type Ia supernovae (SNIa) and low mass type II supernovae (SNII). Thin disc AMR has a considerable scatter. The scatter is larger than that expected from observational errors. Thin disc star seems to appear at the beginning of the Galaxy formation although we are not sure of this feature because such stars have large errors in age determination due to heavy crowding of main sequence isochrones.

For thin disc stars, general trends of the AMR are apparently inconsistent with those previously derived by Twarog (1980), Edvardsson et al. (1993), and Ng & Bertelli (1998). In our data, the mean metallicity is almost constant from 14 Gyr to 1 Gyr and the scatter along the AMR decrease towards younger stars while the mean metallicity increases gradually from [Fe/H] = −0.8 at 16 Gyr to [Fe/H] = −0.1 at the present in the previous researches. Since the Edvardsson et al.'s AMR includes thick disc and halo stars in these previous researches, however, the direct comparison is not appropriate. We carefully examined, therefore, both orbits and the AMR of Edvardsson et al. (1993). Figure 6 shows the AMR by Edvardsson et al. (1993) for thin disc stars according to the criteria given in Sect. 2.2.2. We see that a similar feature is already seen in Edvardsson et al. (1993) if we consider the stars younger than 10 Gyrs. For the stars older than 10 Gyrs, our AMR includes more metal rich stars than that of Edvardsson et al. (1993), and yet it would be difficult to discuss this difference in detail because the age determination of these old stars contains larger errors than younger stars and the number of the sample stars of Edvardsson et al. (1993) is not adequate. There are several features that were not clearly seen in Edvardsson et al.'s AMR: a) the upper envelope of the AMR is remarkably flat at a level similar to the solar metallicity ([Fe/H] $\simeq$ 0.0−0.1) for all times from 14 Gyr to 1 Gyr; and b) although the AMR tends to converge on the point [Fe/H] $\simeq$ +0.3 at 1.6 Gyr in the Edvardsson et al. (1993's) AMR, we found that a fairly large scatter in [Fe/H] still exists even at 1 Gyr.

3.2. The abundance pattern of thin disc

Figure 7 shows the [Ca/Fe] – [Fe/H] relation for thin disc stars. The line represents the GCE model by Pagel & Tautvaišienė (1995). This model predicts that [Ca/Fe] $\simeq$ 0.3 for [Fe/H] $<$ −1.2 (only SNII contribute for metal production) and that [Ca/Fe] decreases as [Fe/H] increases because of iron production from SNIa. The model shows good agreement with the average value of our data. Namely, our data shows the correlation that the more iron-rich stars show smaller [Ca/Fe]. The dispersion of [Ca/Fe] along the model line is, however, larger than that expected from the uncertainty of observation. The scatters among the age, [Fe/H], and [Ca/Fe] are discussed in Sect. 5.5.

Table 2. The sample stars with spectroscopic [Fe/H] observation. Only available at CDS.

Table 3. The sample stars with *ubvy*-Hβ photometry. Only available at CDS.

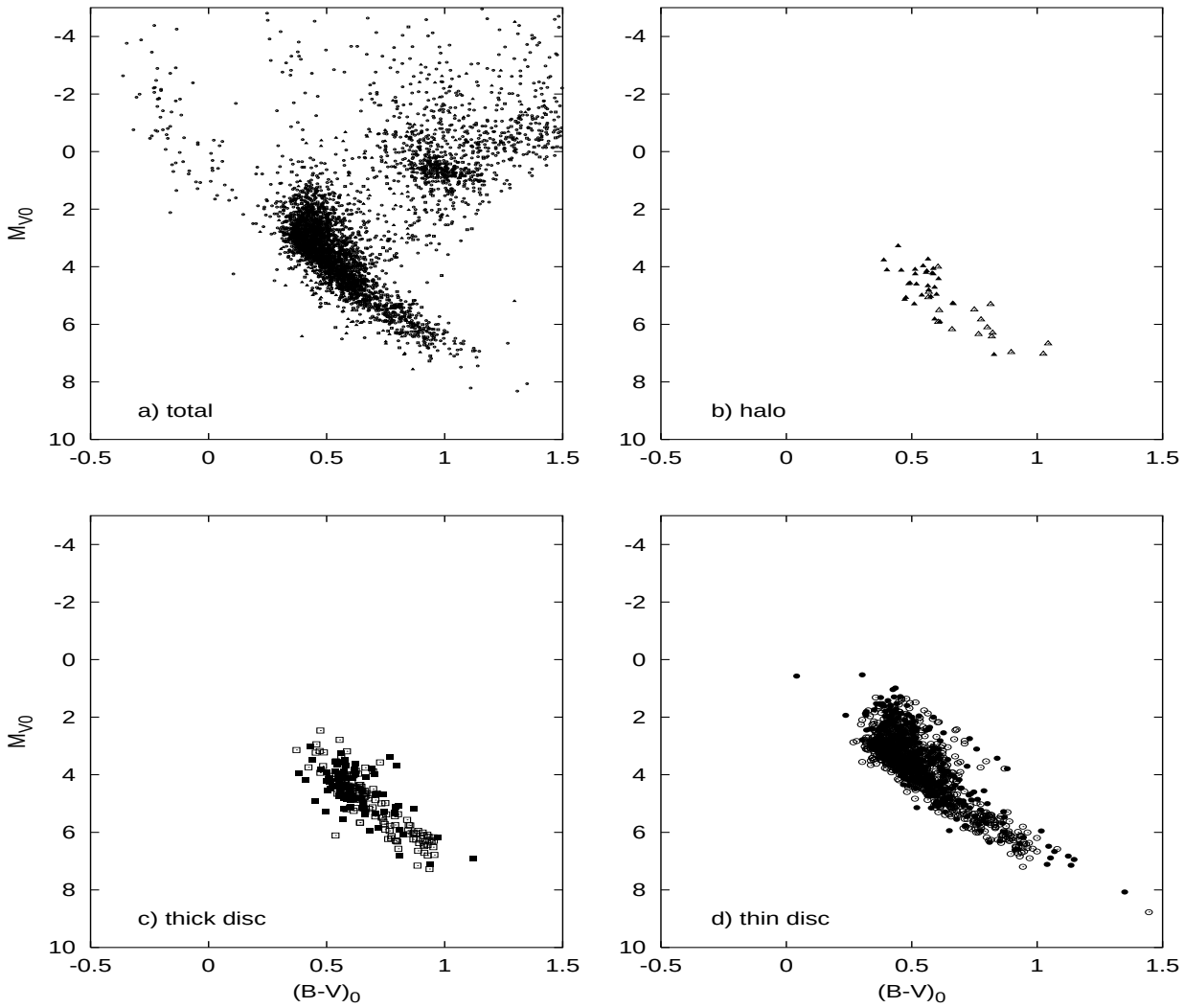

Fig. 3. Colour-magnitude diagram for the sample stars. **a)** 4240 stars before sample selection. **b)–d)** the selected samples. Filled symbols represent the star with spectroscopic data, while open symbols represent stars with photometric data. Circles, squares and triangles represent thin disc, thick disc and halo stars, respectively.

4. The thick disc

4.1. The thick disc AMR

Figure 8 presents the spectroscopic AMR and the photometric AMR for thick disc. We realise three features, i.e.,

1) The bulk of thick disc stars are older than 5 Gyr. The average age of thick disc stars is 8.2 Gyr. The AMR suggests that the star formation in thick disc stopped almost 8.2 Gyr ago;
2) The mean metallicity of thick disc stars is $\langle$ [Fe/H] $\rangle \sim -0.5$ and the spread in [Fe/H] ranges from [Fe/H] = -1.0 to solar. This feature is consistent with previous research (Gilmore & Wyse 1985; Carney et al. 1989; Layden 1995a, b);
3) The scatter along the AMR is larger than that for a thin disc.

4.2. The abundance pattern of thick disc

Figure 9 shows the [Ca/Fe] – [Fe/H] diagram for thick disc stars. The dotted line in Fig. 9 represents the best fit model for the chemical evolution for outer thin disc by Pagel & Tautvaišienė (1995). Clearly, Fig. 9 shows that the thick disc stars are more α-enhanced than the thin disc stars at the same [Fe/H] value.

This trend has been reported by Gratton et al. (2000) and Prochaska et al. (2000). Prochaska et al. (2000) suggested that α-enhancement in the thick disc indicates that the thin disc stars formed from gas more polluted by SNIa, which suggests that the thin disc formation is significantly delayed (>1 Gyr) from the thick disc formation. We could not find, however, any clear evidence for delayed thick disc formation from the AMRs of thin disc and thick disc stars. Interestingly, bulge

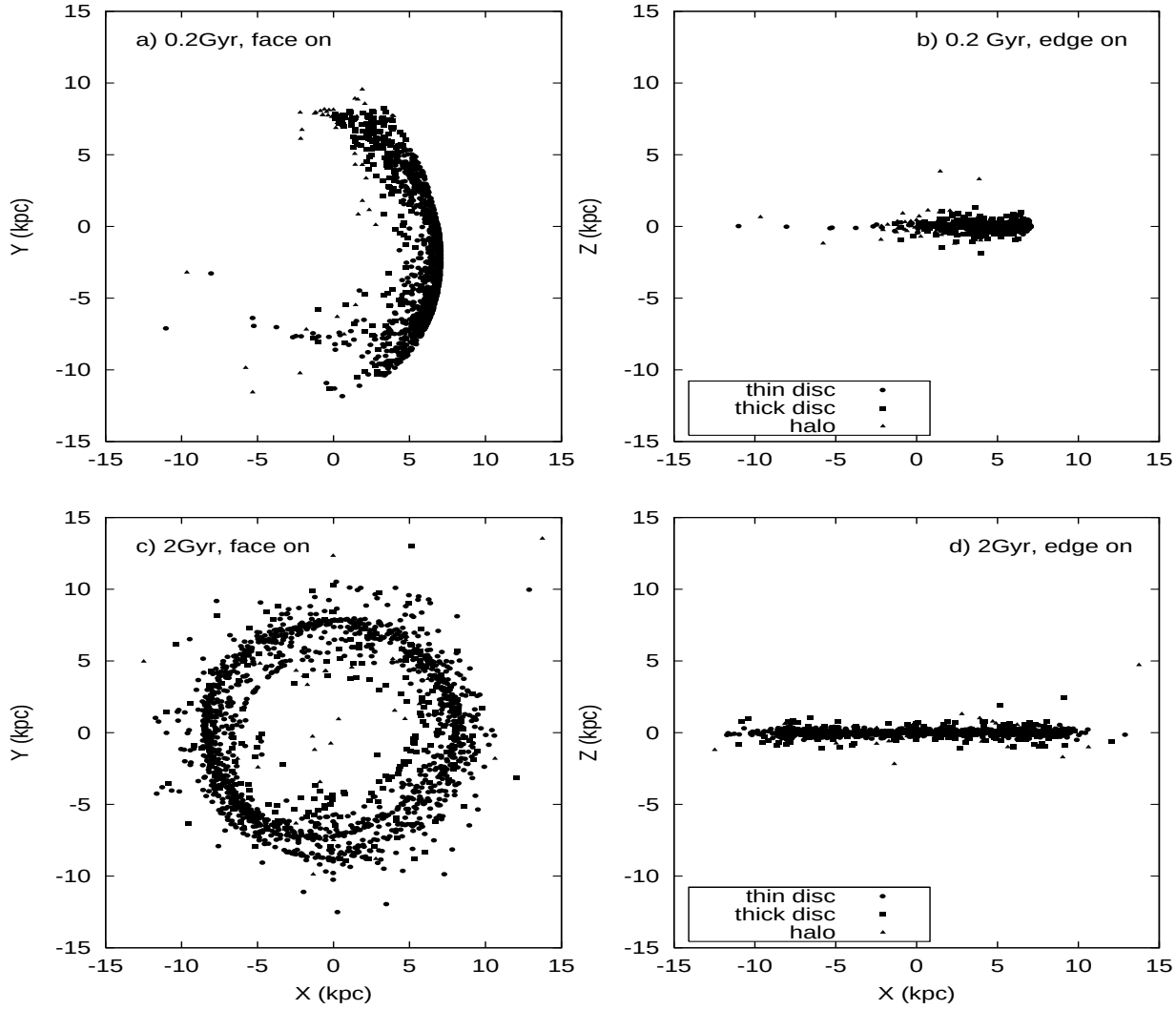

Fig. 4. Snapshot of the orbits of our sample stars. **a)** and **b)** the positions of stars of 0.2 Gyr ago. **c)** and **d)** these of 2 Gyr ago. The left panels are face on views and the right panels are edge on views.

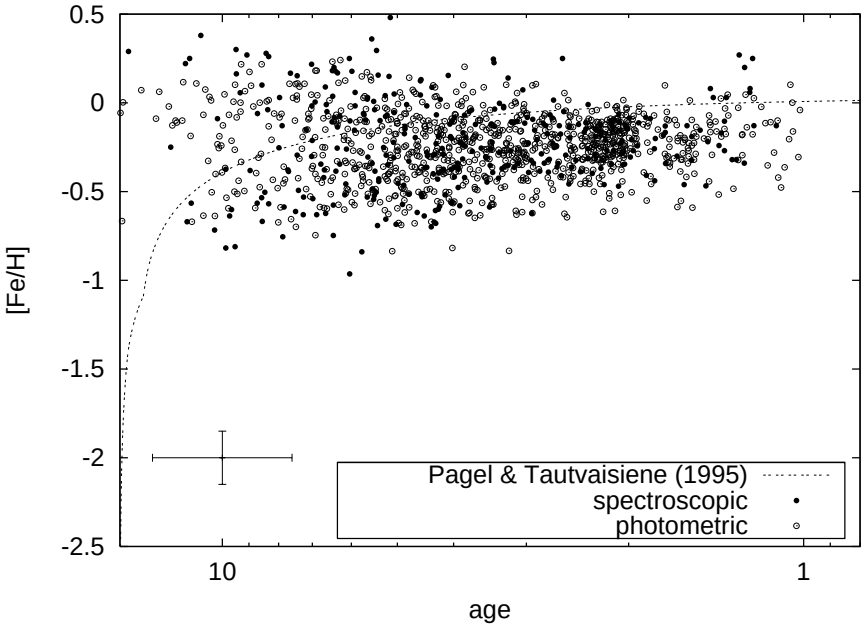

Fig. 5. The spectroscopic and photometric AMR for thin disc stars.

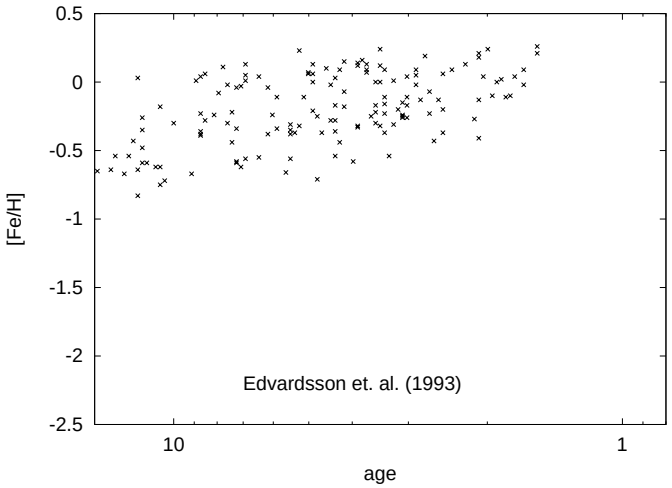

Fig. 6. The photometric AMR for thin disc stars by Edvardsson et al. (1993).

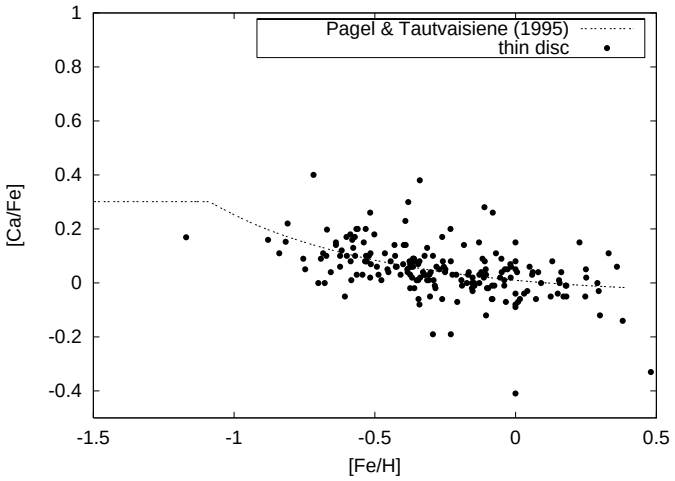

Fig. 7. The [Ca/Fe] – [Fe/H] diagram for thin disc stars.

stars of the Galaxies show a similar trend of α-enhancement and are believed to have experienced rapid star formation history (McWilliam & Rich 1994; Rich & McWilliam 2000). The α-enhancement of thick disc stars, therefore, may be also understood as the result of the rapid star formation.

5. Discussion

5.1. Uncertainty in the AMR

5.1.1. Inhomogeneity of spectroscopic [Fe/H] data

Unfortunately, our AMR contains large errors in metallicity; typically $\epsilon_{[\mathrm{Fe/H}]} = 0.15$ dex due to inhomogeneous data taken from different authors, while $\epsilon_{[\mathrm{Fe/H}]} = 0.1$ dex in Edvardsson et al. (1993) due to their homogeneous [Fe/H] data reduced by the same analysis method. Even if stellar spectra were taken with high S/N and high resolution, [Fe/H] estimates by different authors could result in large scatter in [Fe/H].

Therefore, without examining carefully the details of individual analyses to understand the differences, it would be dangerous to argue too much details of the value of metallicity. We also have to keep in mind that [Fe/H] determinations are affected by the adopted effective temperatures, gravities and microturbulent velocities, and that a stellar metal abundance can be in error, even if the observations are of excellent quality (Cayrel de Strobel et al. 1997).

However, recent observations are in good agreement for different observers. We have studied the most observed 30 stars in the [Fe/H] catalogue to find that the average dispersion in metallicity is 0.13 dex (see Table 4). Our sample includes extremely metal-deficient stars, in which the dispersion in metallicity tends to show larger values. The dispersion in the metallicity for stars with [Fe/H] > -2.5 is even smaller. Considering that the our sample includes a very small number of extremely metal-deficient stars, we conclude that the dispersion in the metallicity can be estimated to be 0.11 dex.

5.1.2. Uncertainty in the age

Uncertainties in $M_{V_0}, (B-V)_0$ and Z cause errors for resulting ages. Errors in M_{V0} and $(B-V)_0$ are typically 0.2 mag ($\simeq$10% in parallax) and 0.02 mag in our data. Combined with Z uncertainties, we can determine the expected error in the resulting age. The errors in ages also depends on the initial mass of the stars through their position of colour-magnitude diagram and the nature of the isochrones hereon. We conducted, therefore, Monte Carlo simulations assuming the AMR and the star formation history in the one zone infall model of Pagel & Tautvaišienė (1995). We took the set of stars (the simple stellar population) from 15 Gyr old to the present, with given metallicity from AMR and star formation history of Pagel & Tautvaišienė (1995). The locations on the colour-magnitude diagram are derived from Yi et al. (2001), adding Gaussian errors of $M_{V_0}, (B-V)_0$ and Z. Then we obtained the age by using the same method in Sect. 2.2. Figure 10 shows the resulting AMR with errors of 0.07 in Z (left) and 0.13 in Z (right). Notably, the expected spread in age – due only to errors – shown by both panels of Fig. 10 is smaller than the observed dispersion of points in Fig. 5 for stars older than 3 Gyr.

5.2. Abundance gradient

In order to discuss the radial abundance gradient of the Galaxy, it is not appropriate to use the present position of the stars as mean position of the stellar orbit. We used, instead, $R \equiv (R_\mathrm{p} + R_\mathrm{a})/2$, for the distance from the Galactic centre (Edvardsson et al. 1993). We also employed z_max for the characteristic distance from the Galactic plane.

5.2.1. Thin disc abundance gradient

Figure 11 presents the [Fe/H]–R relation for thin disc stars. Filled symbols represent spectroscopic data while empty symbols show photometric data. Both spectroscopic and photometric data show no strong correlation between R and [Fe/H]. The line are the observations derived by Díaz (1989). Figure 12 shows the [Fe/H] – z_max relation for thin disc stars. These data also show no strong correlations.

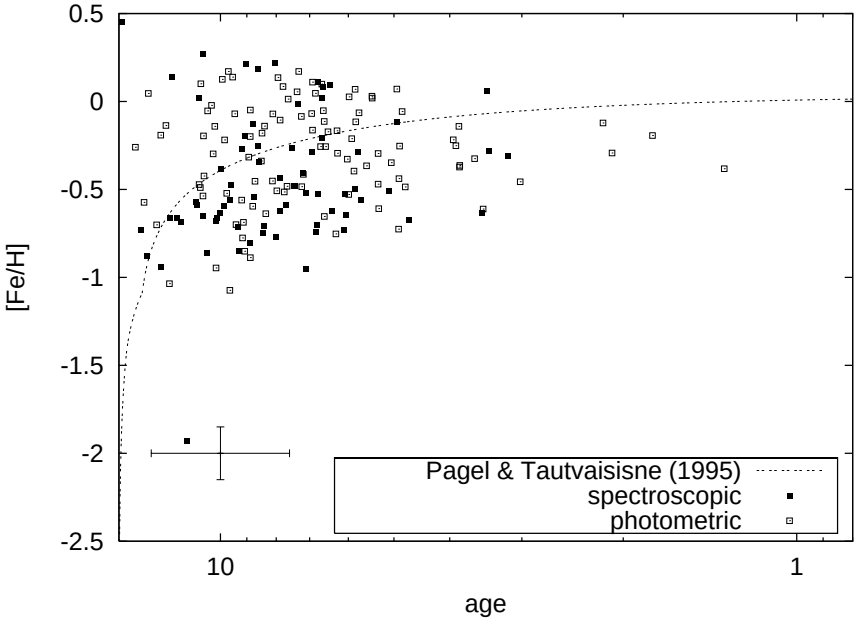

Fig. 8. The spectroscopic and photometric AMR for thick disc stars.

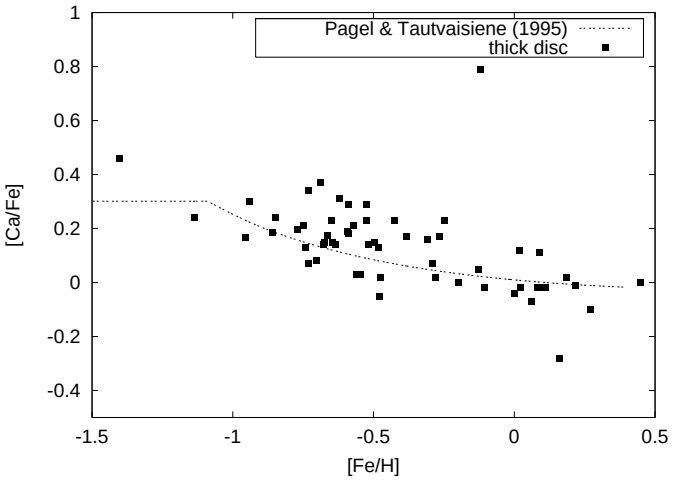

Fig. 9. The [Ca/Fe] – [Fe/H] diagram for thick disc stars.

5.2.2. Thick disc abundance gradient

Figure 13 represents the [Fe/H]–R relation for thick disc stars. Filled symbols represent spectroscopic data, while empty ones represent photometric data. Both spectroscopic and photometric data show little correlation between R and [Fe/H]. Figure 14 shows the [Fe/H]–$z_{\max}$ relation for thick disc stars. Unlike thin disc stars, thick disc stars show the feature that the stars more distant from the Galactic plate tend to be more metal poor. Namely, a vertical abundance gradient is seen in thick disc. Comparing the thin disc stars and thick disc stars with 100 pc $< z_{\max} <$ 600 pc, the thick disc stars are clearly more metal-deficient than the thin disc stars. This phenomenon is naturally understood if we surmise that these two kinds of stellar groups have a different origin: the thick disc stars located at the distance $z_{\max} > 100$ pc formed intrinsically in the region distant from the Galactic plane while the thin disc stars formed near the Galactic plane and drifted or heated-up vertically to 100 pc away from their original birth place.

5.3. The G-dwarf problem

Figure 15 shows the metallicity distribution function for thin disc stars and thick disc stars. Although it is impossible to discuss the property of the abundance distribution because our sample lacks completeness, it is clear that both thin disc and thick disc are deficient in metal-poor stars. Notably, the G-dwarf problem does exist for thick disc stars. Since the metallicity distribution function of metal-deficient halo stars can be explained by simple model (Laird et al. 1988), a thick disc presents a striking contrast to halo, that abundance distribution functions for thick disc stars shows rather close features to that of bulge (McWilliam & Rich 1994).

5.4. Formation process for thick disc

We here discuss how a thick disc formed in the Galaxy. In summary, a thick disc shows three important features, i.e. 1) thick disc stars are older than 5 Gyr, 2) thick disc stars show vertical abundance gradients, and 3) thick disc stars have different abundance patterns compared with thin disc counterparts. To date, thick disc formation scenarios, such as monolithic collapse (Larson 1976; Jones & Wyse 1983), dynamical heating (Noguchi 1998), major merger, and accretion of dwarf galaxies (Quinn & Goodman 1986) have been proposed.

Major merger should invoke a strong peak in age-distribution. It is also widely believed that merger will work as reducing the vertical abundance gradient. Our research does not, therefore, support the thick disc formation with major merger. If a thick disc is formed from heating of the thin disc, the star formation history of a thick disc should be similar to that of the thin disc and the similar star formation history essentially produces the similar [Ca/Fe]–[Fe/H] relation.

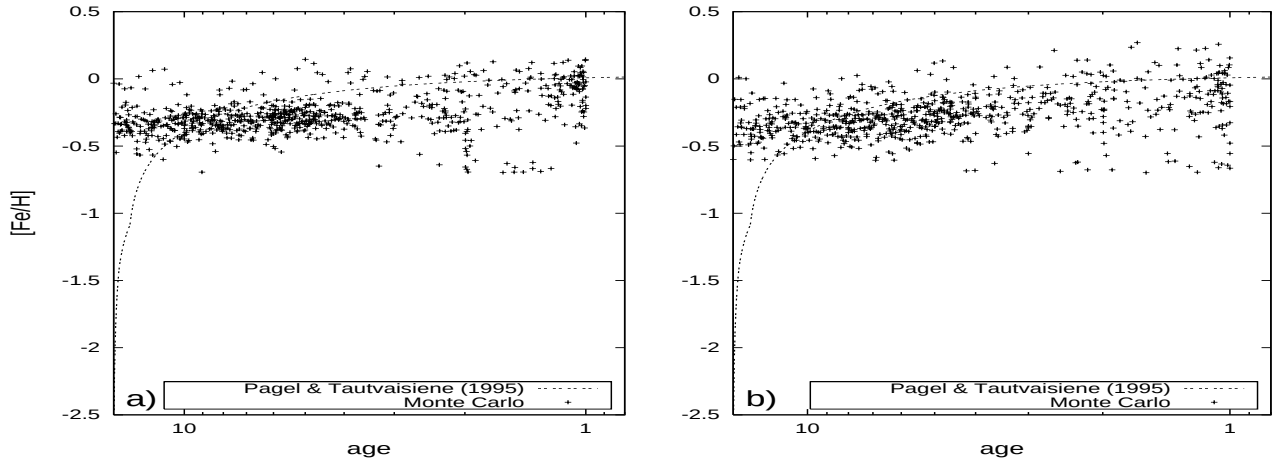

Fig. 10. The simulated AMR from one zone infall model by Pagel & Tautvaišienė (1995). **a)** The errors in Z are set to be 0.07. **b)** These are set to be 0.13. The errors in M_{V_0} and $(B-V)_0$ are 0.2 mag and 0.02 mag in both figures.

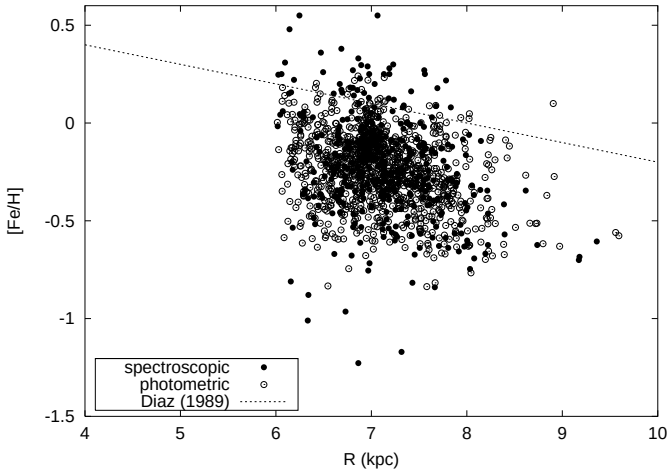

Fig. 11. The [Fe/H]–R relation for thin disc stars. Dashed line represents observations of H II regions (Díaz 1989).

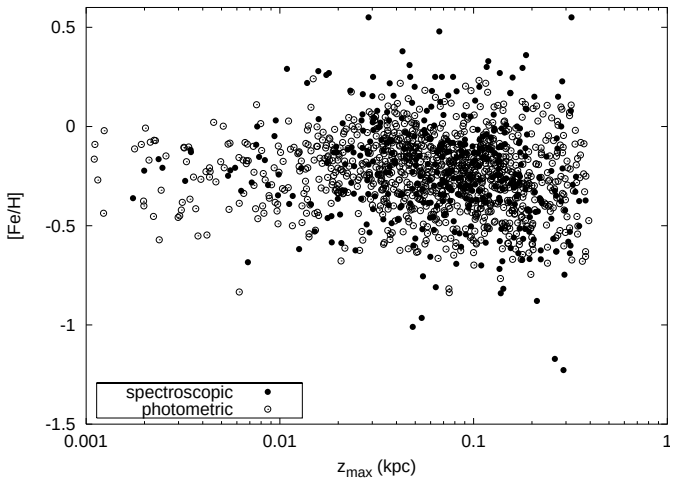

Fig. 12. The [Fe/H]–$z_{\max}$ relation for thin disc stars.

A heating mechanism is, therefore, unlikely to explain the thick disc formation. The other two theories both account for our result.

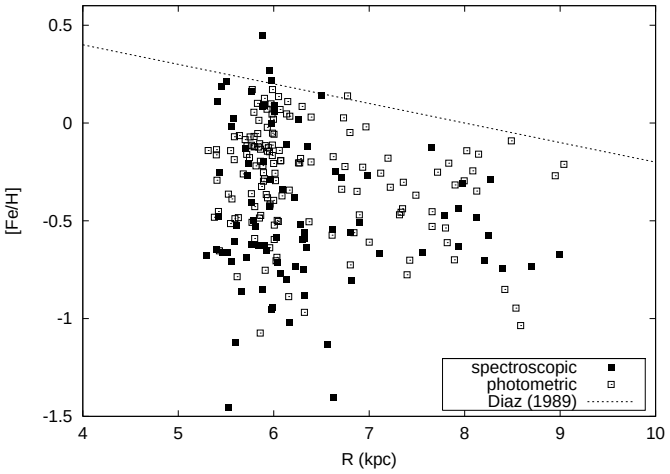

Fig. 13. The [Fe/H]–R relation for thick disc stars. Dashed line represents observations of H II regions (Díaz 1989).

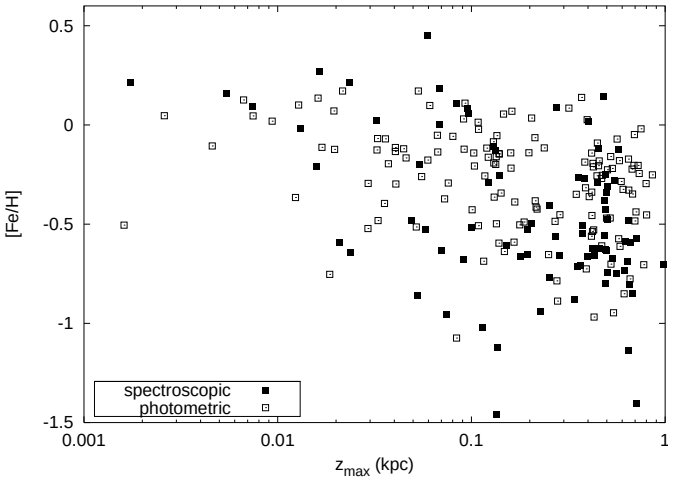

Fig. 14. The [Fe/H]–$z_{\max}$ relation for thick disc stars.

5.5. Scatter in the AMR for thin disc

In this section, we will try to explain the scatter along the AMR by simple extension of the one zone model derived by Pagel & Tautvaišienė (1995).

Table 4. Differences of [Fe/H] values with different observations.

Name	Number of obs.	[Fe/H] $_{\rm average}$	[Fe/H]$_{\rm max}$	[Fe/H]$_{\rm min}$	$\epsilon_{\rm [Fe/H]}$
CD −38 245	8	−3.95	−4.42	−3.00	0.39
HD 122563	16	−2.69	−2.93	−2.45	0.10
BD +03 740	11	−2.66	−2.98	−2.3	0.22
HD 140283	26	−2.49	−2.75	−2.21	0.14
BD +2 3375	10	−2.28	−2.65	−1.95	0.19
HD 216143	9	−2.21	−2.26	−2.10	0.05
HD 128279	9	−2.19	−2.50	−1.97	0.16
HD 165195	11	−2.18	−2.26	−1.92	0.09
HD 84937	12	−2.14	−2.43	−1.86	0.17
BD +37 1458	9	−2.02	−2.33	−1.79	0.19
HD 19445	19	−2.00	−2.31	−1.76	0.14
HD 187111	13	−1.78	−2.35	−1.54	0.19
HD 26297	10	−1.77	−1.87	−1.68	0.06
HD 122956	13	−1.75	−1.96	−1.53	0.10
HD 64090	12	−1.68	−1.94	−1.49	0.16
HD 211998	10	−1.53	−1.68	−1.25	0.14
HD 83212	11	−1.46	−1.57	−1.37	0.06
HD 94028	11	−1.44	−1.66	−1.31	0.12
HD 103095	15	−1.34	−1.59	−1.17	0.11
HD 194598	17	−1.14	−1.37	−0.99	0.11
HD 201891	15	−1.01	−1.12	−0.87	0.06
HD 76932	14	−0.92	−1.05	−0.76	0.09
HD 63077	15	−0.89	−1.16	−0.53	0.16
HD 022879	12	−0.86	−0.99	−0.76	0.05
HD 59984	14	−0.82	−1.60	−0.52	0.24
HD 124897	14	−0.54	−0.69	−0.37	0.10
HD 61421	13	−0.02	−0.18	0.05	0.05
HD 9826	8	0.09	−0.03	0.17	0.05
HD 217014	8	0.15	0.05	0.21	0.07
HD 128620	10	0.19	0.10	0.25	0.04

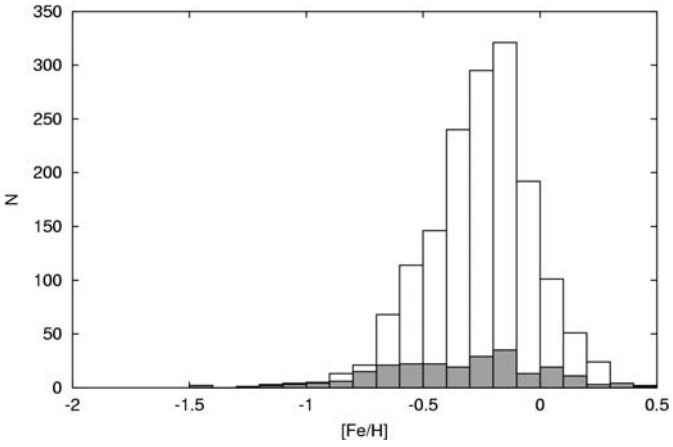

Fig. 15. Abundance distribution function for thin disc (open boxes) and thick disc (gray boxes).

5.5.1. Metallicity-orbit relation

The solar neighbourhood stars consist of a mixture of stars born at different places with different orbits. This fact may account for the scatter along the thin disc AMR (Edvardsson et al. 1993; Pagel & Tautvaišienė 1995; Prantzos & Boissier 2000). As already seen in Sect. 5.2, the abundance gradient is not significant for thin disc stars. Another relations between orbital elements and metallicity relation may exist for thin disc stars. For example, if we find for the metallicity-orbit relation that stars with larger eccentricity tend to be more metal-deficient, the scatter along the AMR can be attributed to such a relation. Therefore, we examined the U, V, W, e – [Fe/H] relation (Fig. 16). All of these relations, however, show more a scattered feature than a strong correlation. Notably, a large scatter in [Fe/H] is seen even if the stars with the same orbital parameters are selected. The scatter along the AMR cannot, therefore, be attributed to a relation of this kind.

5.5.2. Inhomogeneous effective yield and star formation

The effective yield can be different from place to place although the true yield is homogeneous, because the supernova ejecta are inhomogeneous due to axisymmetric explosions

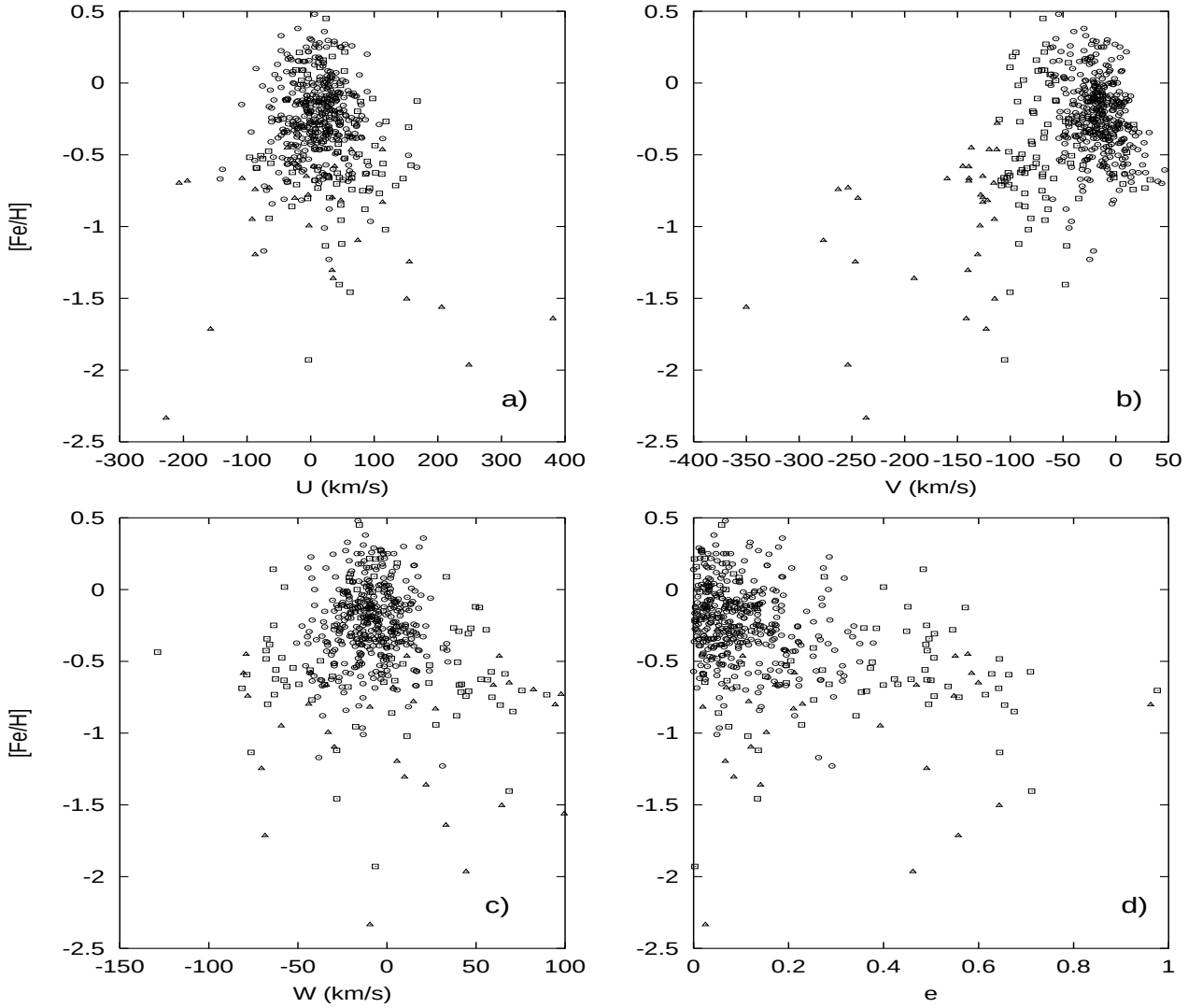

Fig. 16. a) U – [Fe/H] relation. **b)** V–[Fe/H]. **c)** W–[Fe/H]. **d)** e–[Fe/H]. Circles, squares, and triangles represent thin disc, thick disc, and halo stars, respectively.

of rotating massive stars (Maeda et al. 2001). Even if the explosions are isotropic, the ejecta may stochastically contaminate the surroundings, unless the ISM is distributed uniformly. The scatter can be explained even if the star formation history in the "solar torus" is completely homogeneous. It is also possible that the local inhomogeneity of the star formation rate produces the scatter. To examine these scenarios, we prepared 7 models by modifying the parameters in the analytical model of Pagel & Tautvaišienė (1995). Table 5 shows the adopted parameters for each model. Model A is an original infall model taken from Pagel & Tautvaišienė (1995). Model B and C assumed twice and half yield SNII ejecta, respectively. SNIa yield and star formation timescale is changed in model D, E and model F, G in the same manner.

The scatter may arise if relative contributions of SNIa and SNII differ from place to place. The various panels of Fig. 17 show the AMR, age–[Ca/Fe] relation, and the [Ca/Fe]–[Fe/H] diagram with models A, B, and C. Clearly the difference in the effective yield of SNII produces smaller scatter along the AMR than the observations, while the scatter in the [Ca/Fe]–[Fe/H] diagram (right) is too large to explain the observations.

Table 5. The parameters for 7 GCE models, originally introduced by Pagel & Tautvaišienė (1995). $1/\omega$ represent the star formation timescale.

model	ω	$y_{\mathrm{Fe,SNIa}}$	$y_{\mathrm{Fe,SNII}}$	$y_{\mathrm{Ca,SNIa}}$	$y_{\mathrm{Ca,SNII}}$
A	0.3	0.42	0.28	0.18	0.56
B	0.3	0.42	0.56	0.18	1.12
C	0.3	0.42	0.14	0.18	0.28
D	0.3	0.84	0.28	0.36	0.56
E	0.3	0.21	0.28	0.09	0.56
F	0.15	0.42	0.28	0.18	0.56
G	0.6	0.42	0.28	0.18	0.56

Next, we examined the inhomogeneous effective yield of SNIa. Figure 18 show the models with different effective yields for SNIa. Models A, D, and E reproduce fairly well both the trend of thin disc stars' AMR and the scatter along it. However,

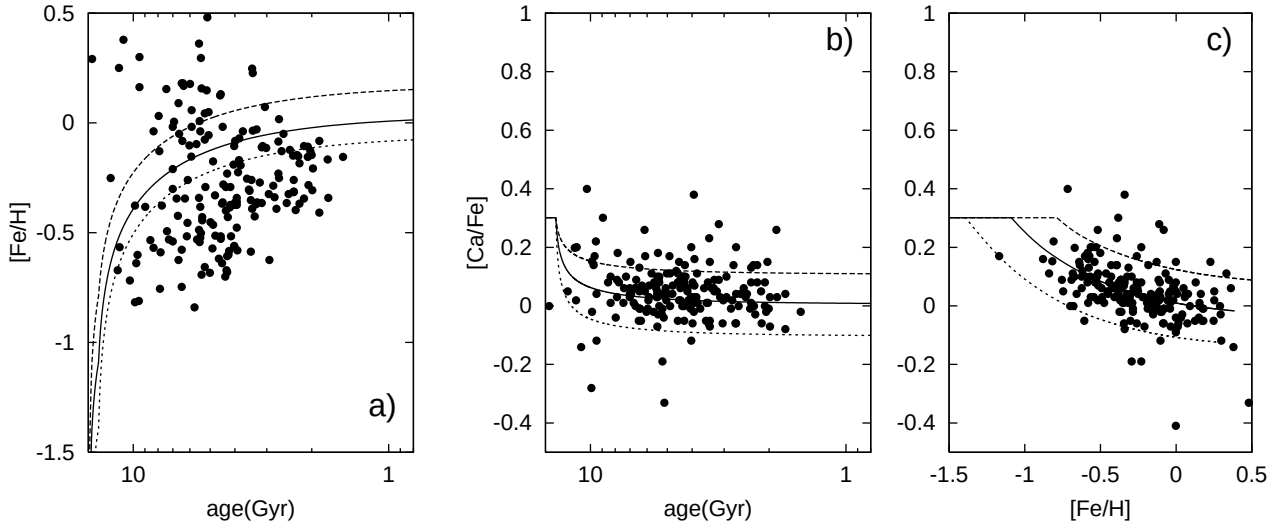

Fig. 17. Comparison of **a)** the AMR, **b)** age–[Ca/Fe] relation, and **c)** [Ca/Fe]–[Fe/H] diagram with models A (solid line), B (long dashed line), and C (short dashed line).

dividing the [Fe/H] relation into two parts (Fig. 19), metal rich stars and metal poor stars, and examining the [Ca/Fe] –[Fe/H] diagram in detail, we found that this model cannot acount for the scatters. In Fig. 19 the sample stars are divided into two parts. More iron rich stars than model A are designated in circles while metal poor stars are in triangles. Model D and E predict that iron rich stars (circles) will show smaller [Ca/Fe] than model A in Fig. 19 and that the metal poor stars (triangles) will show larger [Ca/Fe] than model A. In our data, however, both iron rich stars and iron poor stars are distributed along model A and show no clear split of [Ca/Fe] in Fig. 19. Thus, models with different effective yield for SNIa cannot explain this feature on the [Ca/Fe] – [Fe/H] diagram.

Finally, the inhomogeneity of star formation rate is examined. Figure 20 shows the models with different star formation rates. The scatter along the age–[Ca/Fe] relation is cleary larger than expected from the models.

Comparing these three hypotheses and our data, we conclude that such a simple modification of one-zone model cannot explain the scatter along the AMR, age–[Ca/Fe] relation, and [Ca/Fe]–[Fe/H] relation simultaneously.

5.5.3. Planet migration

There is growing evidence that the star formation mechanism may have some influence on the metallicity of the star: in particular, Gonzalez (1997) has recently suggested that stars with planets are systematically more metal-rich than stars without planets, and that this is due to the presence of planets ("planet migration"). This effect can cause the scatter in the AMR. Our data include, however, only 14 discovered planet host stars (Mayor & Queloz 1995; Fischer et al. 1999; Butler et al. 2000; Henry et al. 2000; Korzennik et al. 2000; Marcy et al. 2000; Mazeh et al. 2000; Udry et al. 2000; Vogt et al. 2000; Butler et al. 2001; Fischer et al. 2001; Gonzalez et al. 2001; Tinney et al. 2001), and we have scatter in the AMR when we consider only stars without planets. Figure 21 shows the AMR with known planets host stars and other stars. As already noted by Gonzalez (1997) the planets host stars tend to have larger metallicities than the general trend of the AMR. It should be noted that the Sun also shows this "over-metallicity". It seems that the idea is reasonable because the "over-metallcity" of 0.1 dex in [Fe/H] result in the underestimate of the age of ∼1 Gyr. If we consider that ages and [Fe/H] of planet's host stars are underestimated and oversetimated, respectively, the original [Fe/H] and ages of planet's stars shows better fit to the one-zone AMR model. However, it is insufficient or even dangerous to study the general nature of the scatter of the AMR from such a small number of stars (less than 1% of the total samples stars) and we cannot conclude yet that the planet migration is the major cause for the scatter along the AMR.

6. Summary and conclusion

The AMR and orbital parameters are newly derived for 1658 solar neighbourhood stars to which accurate distances are measured by the *HIPPARCOS* satellite. The sample stars are divided into 1382 thin disc stars, 229 thick disc stars, and 47 halo stars according to their orbital parameters. Notably, the thin disc AMR shows a considerable scatter along the one-zone GCE model. No clear relation between orbit and metallicity are found. Namely, the scatter along the AMR exists even if the stars with the same orbits are selected. We examined simple extension of the one-zone GCE models which account for i) inhomogeneity in the effective yield caused by the spatially localised mixing of inter stellar medium; and ii) inhomogeneous star formation history. We found both extensions of one-zone GCE model cannot account for the scatter in age – [Fe/H] – [Ca/Fe] relation simultaneously. In our work, the scatter along the AMR for thin disc stars have been confirmed for far larger samples (1382 stars), which is more than 5 times larger than that used in the previous work of Edvardsson et al. (1993).

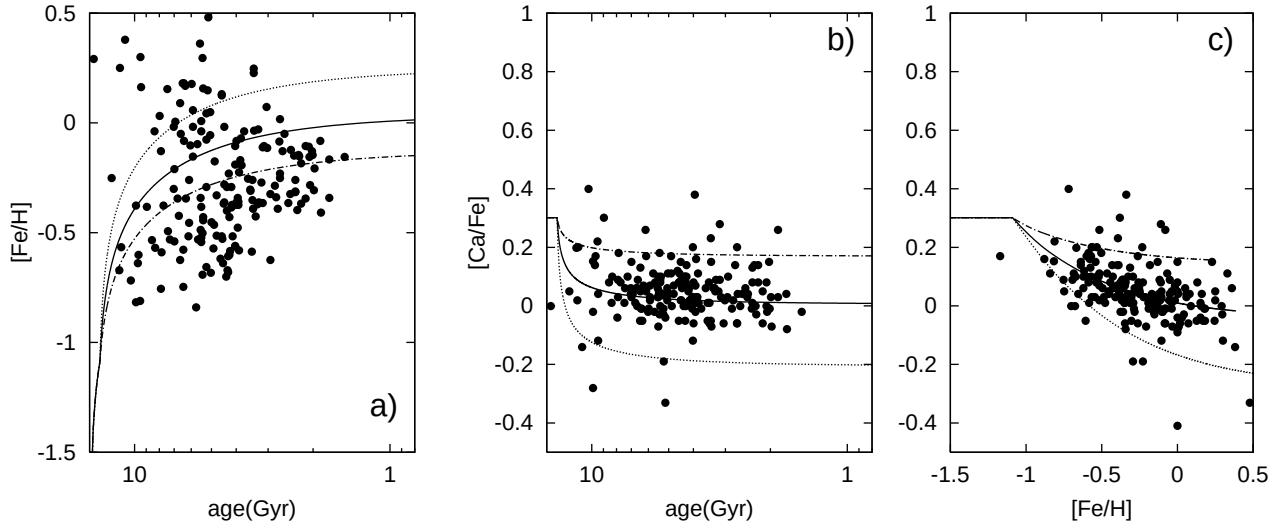

Fig. 18. Comparison of **a)** the AMR, **b)** age–[Ca/Fe] relation, and **c)** [Ca/Fe]–[Fe/H] diagram with models A (solid line), D (dotted line), and E (dash-dotted line).

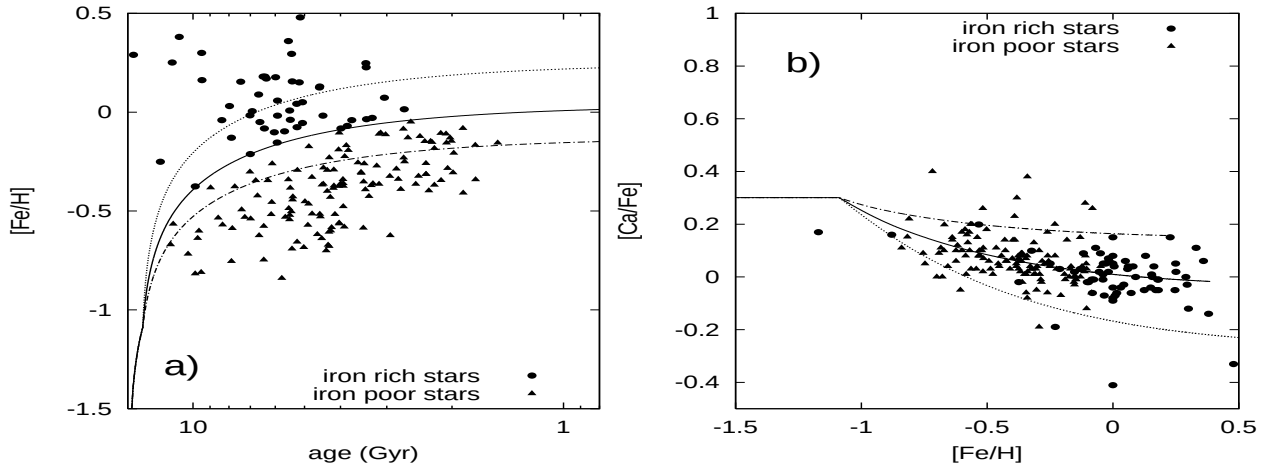

Fig. 19. Comparison of **a)** the AMR and **b)** the [Ca/Fe] diagram in detail. Circles represent stars more iron rich than the model A, while triangles represent iron poor stars.

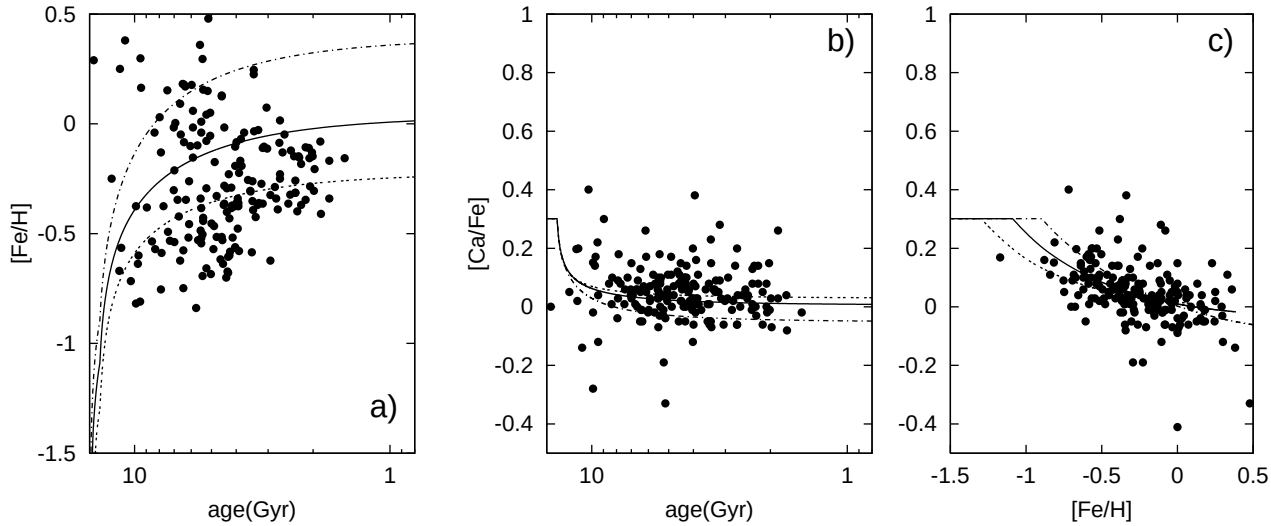

Fig. 20. Comparison of **a)** the AMR, **b)** age–[Ca/Fe] relation, and **c)** [Ca/Fe]–[Fe/H] diagram with models A (solid line), F (dash-dotted line), and G (short dashed line).

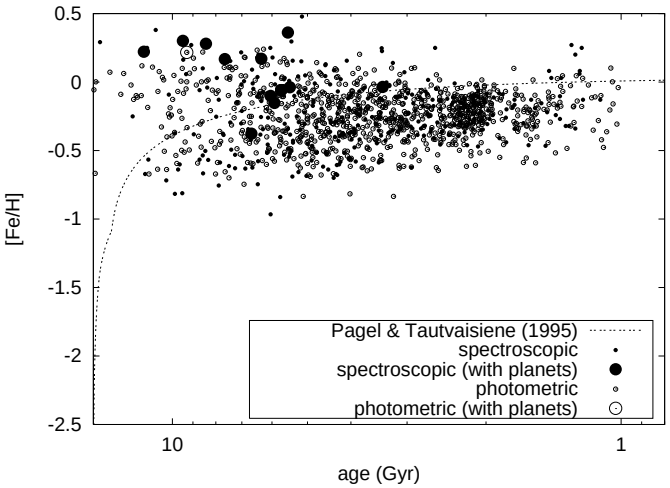

Fig. 21. The AMR and planets hosting stars in our sample. Large symbols denote known planets host stars.

We concluded that this scatter, which should be accounted for by any Galaxy model, is one of the most important features in the formation and evolution of the Galaxy. On the other hand, the AMR for thick disc stars shows that the star formation terminated 8 Gyr ago in the thick disc. We reconfirmed the trend that the thick disc stars are more Ca-rich than the disc stars with the same [Fe/H], which has been already reported by Gratton et al. (2000) and Prochaska et al. (2000). Thick disc stars show a vertical abundance gradient. These three facts, the AMR, vertical gradient, and [Ca/Fe]–[Fe/H] relation, support monolithic collapse and/or accretion of satellite dwarf galaxies as a thick disc formation scenario.

Acknowledgements. We are grateful to the anonymous referee whose suggestions on the early version greatly improved the paper. We thank to Dr. Chiaki Kobayashi for useful discussions. A.I. thanks the Japan Society for Promotion of Science (JSPS) Research Fellowships for Young Scientists.

References

Abia, C., Rebolo, R., Beckman, J. E., & Crivellari, L. 1988, A&A, 206, 100
Arenou, F., Grenon, M., & Gómez, A. 1992, A&A, 258, 104
Barbier-Brossat, M., Petit, M., & Figon, P. 1994, A&AS, 108, 603
Berthet, S. 1991, A&A, 251, 171
Beveridge, C. E., & Sneden, C. 1994, AJ, 108, 285
Boesgaard, A. M., & Tripicco, M. J. 1986, ApJ, 303, 724
Butler, R. P., Tinney, C. G., Marcy, G. W., et al. 2001, ApJ, 555, 410
Butler, R. P., Vogt, S. S., Marcy, G. W., et al. 2000, ApJ, 545, 504
Carlberg, R. G., Dawson, P. C., Hsu, T., & VandenBerg, D. A. 1985, ApJ, 294, 674
Carney, B. W., Latham, D. W., & Laird, J. B. 1989, AJ, 97, 423
Carney, B. W., Wright, J. S., Sneden, C., et al. 1997, AJ, 114, 363
Carretta, E., Gratton, R., Clementini, G., & Pecci, F. F. 1999, in Harmonizing Cosmic Distance Scales in a Post-HIPPARCOS era, ed. D. Egret, & A. Heck, ASP Conf. Ser., 167, 255
Castro, S., Rich, R. M., Grenon, M., Barbuy, B., & McCarthy, J. K. 1997, AJ, 114, 376
Cayrel de Strobel, G., & Bentolila, C. 1989, A&A, 211, 324
Cayrel de Strobel, G., Crifo, F., Lebgreton, Y., & Soubiran, C. 1997, A&AS, 124, 299
Cayrel de Strobel, G., Soubiran, C., & Ralite, N. 2001, A&A, 373, 159
Chen, Y. Q., Nissen, P. E., Zhao, G., Zhang, H. W., & Benoni, T. 2000, A&AS, 141, 491
Ciardullo, R., & Demarque, P. 1977, Yale Trans., 33
Clementini, G., Gratton, R. G., Carretta, E., & Sneden, C. 1999, MNRAS, 302, 22
Díaz, A. I. 1989, in Evolutionary phenomena in the galaxies (Cambridge Univ. Press), 377
Duflot, M., Figon, P., & Meyssonnier, N. 1995, A&AS, 114, 269
Edvardsson, B., Andersen, J., Gustafsson, B., et al. 1993, A&A, 275, 101
ESA 1997, The Hipparcos and Tycho Catalogues (SP-1200)
Feltzing, S., & Gustafsson, B. 1998, A&AS, 129, 237
Fischer, D. A., Marcy, G. W., Butler, R. P., Vogt, S. S., & Apps, K. 1999, PASP, 111, 50
Fischer, D. A., Marcy, G. W., Butler, R. P., et al. 2001, ApJ, 551, 1107
Fulbright, J. P. 2000, AJ, 120, 1841
Gilmore, G., & Wyse, R. F. G. 1985, AJ, 90, 2015
Giridhar, S., Ferro, A. A., & Parrao, L. 1997, PASP, 109, 1077
Gonzalez, G. 1997, MNRAS, 285, 403
Gonzalez, G. 1998, A&A, 334, 221
Gonzalez, G., & Laws, C. 2000, AJ, 119, 390
Gonzalez, G., Laws, C., Tyagi, S., & Reddy, B. E. 2001, AJ, 121, 432
Gratton, R. G., Carretta, E., Matteucci, F., & Sneden, C. 2000, A&A, 358, 671
Gratton, R. G., & Sneden, C. 1991, A&A, 241, 501
Hartmann, K., & Gehren, T. 1988, A&A, 199, 269
Hauck, B., & Mermilliod, M. 1998, A&AS, 129, 431
Henry, G. W., Marcy, G. W., Butler, R. P., & Vogt, S. S. 2000, ApJ, 529, L41
Jehin, E., Magain, P., Neuforge, C., et al. 1999, A&A, 341, 241
Johnson, D. R. H., & Soderblom, D. R. 1987, AJ, 93, 864
Jones, B. J. T., & Wyse, R. F. G. 1983, A&A, 120, 165
King, J. R., Stephens, A., Goesgaard, A. M., & Deliyannis, C. P. 1998, AJ, 115, 666
Korzennik, S. G., Brown, T. M., Fischer, D. A., Nisenson, P., & Noyes, R. W. 2000, ApJ, 533, L147
Laird, J. B., Carney, B. W., Rupen, M. P., & Latham, D. W. 1988, AJ, 96, 1908
Larson, R. 1976, MNRAS, 176, 31
Layden, A. C. 1995a, AJ, 110, 2288
Layden, A. C. 1995b, AJ, 110, 2312
Lutz, T. E., & Kelker, D. H. 1973, PASP, 85, 573
Maeda, K., Nakamura, T., Nomoto, K., et al. 2001, ApJ, 565, 405
Magain, P. 1989, A&A, 209, 211
Malaroda, S., Levato, H., & Galliani, S. 2001, Complejo Astronomico El Leoncito
Marcy, G. W., Butler, R. P., & Vogt, S. S. 2000, ApJ, 536, L43
Mayor, M., & Queloz, D. 1995, Nature, 378, 355
Mazeh, T., Naef, D., Torres, G., et al. 2000, ApJ, 532, L55
McWilliam, A., & Rich, R. M. 1994, ApJS, 91, 749
Ng, Y. K., & Bertelli, G. 1998, A&A, 329, 943
Nissen, P. E., Gustafsson, B., Edvardsson, B., & Gilmore, G. 1994, A&A, 285, 440
Nissen, P. E., & Schuster, W. J. 1991, A&A, 251, 457

Nissen, P. E., & Schuster, W. J. 1997, A&A, 326, 751
Noguchi, M. 1998, Nature, 392, 253
Pagel, B. E. J., & Tautvaišienė, G. 1995, MNRAS, 276, 505
Pilachowski, C. A., Sneden, C., & Booth, J. 1993, ApJ, 407, 699
Prantzos, N., & Boissier, S. 2000, MNRAS, 313, 338
Prochaska, J. X., Naumov, S. O., Carney, B. W., McWilliam, A., & Wolfe, A. M. 2000, AJ, 120, 2513
Quinn, P., & Goodman, J. 1986, ApJ, 309, 472
Rich, R. M., & McWilliam, A. 2000, in Proc. SPIE 4005, Discoveries and Research Prospects form 8- to 10-Meter-Class Telescopes, ed. J. Bergeron, 150
Sadakane, K., Honda, S., Kawanomoto, S., Takeda, Y., & Takada-Hidai, M. 1999, PASJ, 51, 505
Santos, N. C., Israelian, G., & Mayor, M. 2000, A&A, 363, 228
Schuster, W. J., & Nissen, P. E. 1989, A&A, 221, 65
Smith, V. V., Coleman, H., & Lambert, D. L. 1993, ApJ, 417, 287
Smith, W. W., & Lambert, D. L. 1986, ApJ, 303, 226
Smith, W. W., & Lambert, D. L. 1987, MNRAS, 226, 563
Sofue, Y. 1996, ApJ, 458, 120
Thorén, P., & Feltzing, S. 2000, A&A, 363, 692
Tinney, C. G., Butler, R. P., Marcy, G. W., et al. 2001, ApJ, 551, 507
Tomkin, J., Edvardsson, B., Lambert, D. L., & Gustafsson, B. 1997, A&A, 327, 587
Turon, C., Egret, D., Gomez, A., et al. 1993, Bull. Inf. CDS, 43, 5
Twarog, B. A. 1980, ApJ, 242, 242
Udry, S., Mayor, M., Naef, D., et al. 2000, A&A, 356, 590
VandenBerg, D. A. 1983, ApJS, 51, 29
VandenBerg, D. A. 1985, ApJS, 58, 711
Vogt, S. S., Marcy, G. W., Butler, R. P., & Apps, K. 2000, ApJ, 536, 902
Yi, S., Demarque, P., Kim, Y.-C., et al. 2001, ApJS, 136, 417